ADVANCED FUNCTIONAL MATERIALS
www.afm-journal.de

Co-Assembled and Microfabricated Bioactive Membranes

*Ana C. Mendes, Katherine H. Smith, Esther Tejeda-Montes, Elisabeth Engel, Rui L. Reis, Helena S. Azevedo, and Alvaro Mata**

The fabrication of hierarchical and bioactive self-supporting membranes, which integrate physical and biomolecular elements, using a single-step process that combines molecular self-assembly with soft lithography is reported. A positively charged multidomain peptide (with or without the cell-adhesive sequence arginine-glycine-aspartic acid-serine (RGDS)) self-assembles with hyaluronic acid (HA), an anionic biopolymer. Optimization of the assembling conditions enables the realization of membranes with well-controlled and easily tunable features at multiple size scales including peptide sequence, building-block co-assembly, membrane thickness, bioactive epitope availability, and topographical pattern morphology. Membrane structure, morphology, and bioactivity are investigated according to temperature, assembly time, and variations in the experimental setup. Furthermore, to evaluate the physical and biomolecular signaling of the self-assembled microfabricated membranes, rat mesenchymal stem cells are cultured on membranes exhibiting various densities of RGDS and different topographical patterns. Cell adhesion, spreading, and morphology are significantly affected by the surface topographical patterns and the different concentrations of RGDS. The versatility of the combined bottom-up and top-down fabrication processes described may permit the development of hierarchical macrostructures with precise biomolecular and physical properties and the opportunity to fine tune them with spatiotemporal control.

1. Introduction

As a bottom-up fabrication technique, self-assembly facilitates the development of new biomaterials with molecular resolution by precisely controlling the organization of high quantities of small building-blocks.[1] This level of precision enables the capacity to generate nanoarchitectures similar to those found in the natural extracellular matrix (ECM) that additionally exhibit biomolecular ligands capable of controlling biological processes.[2] However, a major limitation of current self-assembling systems is the lack of structural and functional control at the micro and macroscopic levels, which significantly limits the bulk properties of the material and consequently its practicality, functionality, and overall performance.

In order to overcome this limitation, a number of groups are focusing efforts on developing strategies that facilitate molecular assembly at higher size-scales. One approach relies on molecules that incorporate by design the "code" to guide their assembly across scales. For example, Hartgerink et al. have developed a strategy that employs electrostatic interactions to guide the self-assembly of heterotrimeric triple helices designed to replicate the self-assembly of collagen, from peptide chain to triple helix formation to nanofiber and finally to a hydrogel.[3] Stupp and co-workers have reported the formation of hierarchically structured macroscopic sacs and membranes obtained by the co-assembly of positively charged small peptide molecules (peptide amphiphiles) and a large negatively charged polymer (hyaluronic acid) with a millimeter size scale.[4–6] Another example of hierarchical organization was provided by Chung et al. who used self-templating assembly of chiral colloidal particles (phage particles) to produce long-range ordered supramolecular films.[7] While these mechanisms are highly biomimetic and generate materials with improved macroscopic properties, there is still a great need to develop novel fabrication schemes that reproducibly control molecular assembly at higher scales.

The use of top-down methods to direct multiscale self-assembly is one such approach as there is the potential for high reproducibility, micro/nano precision over large areas, and batch fabrication capabilities.[8] Soft lithography techniques have been widely used to fabricate material surfaces with molecular patterns at various scales.[9] Towards tissue engineering and regenerative medicine applications specifically, these methods have been used to precisely manipulate and localize cells, control cell–cell and cell–substrate interactions, guide cell behavior, and facilitate the fundamental study of many biological

A. C. Mendes, Prof. R. L. Reis, Dr. H. S. Azevedo
Biomaterials, Biodegradables and Biomimetics
University of Minho
Headquarters of the European
Institute of Excellence on Tissue Engineering
and Regenerative Medicine
AvePark, Guimarães, Portugal
ICVS/3B´s, PT Government Associate Laboratory, Braga, Portugal
E-mail: amata@pcb.ub.es
Dr. K. H. Smith, E. Tejeda-Montes, Dr. A. Mata
The Nanotechnology Platform
Parc Científic Barcelona, 08028 Barcelona, Spain
E-mail: amata@pcb.ub.es
Dr. E. Engel
Institut de Bioeginyeria de Catalunya
08028 Barcelona, Spain

DOI: 10.1002/adfm.201201065

processes.[10,11–13] These studies have comprehensibly demonstrated the possibility to modulate cell morphology,[14] adhesion,[15] migration,[16] proliferation,[12,17] and differentiation[18] through precise nano- and microstructures using large variety of biocompatible materials such as polydimethylsiloxane,[12,17] polylactic acid,[19] hyaluronic acid,[20] or poly-ε-caprolactone.[21] Using the soft lithography technique of replica molding in conjunction with a self-assembling peptide amphiphile, Mata et al.,[11] reported on the possibility to enhance osteoblastic differentiation when presenting cells with a combination of bioactive nanofibers and well-defined 40 μm diameter, 4 μm deep holes. The possibility to fabricate materials with such well-defined topographical patterns using increasingly complex self-assembling systems represents an attractive approach to generate biomimetic and easily tunable materials. In addition, the extra level of hierarchical order gained by combining top-down techniques with self-assembly provides a higher level of bioactivity by enabling the opportunity for cell interaction on various size scales.

Synthetic membrane scaffolds would benefit significantly from this kind of top-down/bottom-up approach. In the human body, membranes play critical roles supporting cell attachment and function, regulating nutrient and waste transfer, and providing boundaries between tissues and organs.[22] The possibility of using artificial membranes as in vitro or in vivo scaffolds capable of exhibiting specific signals, tunable properties, and cell guiding features would be broadly useful in tissue engineering and regenerative medicine applications. For example, membranes have been investigated for bone and cartilage regeneration,[23] cornea repair,[24] skin engineering,[25] reconstruction of the abdominal wall,[26] and cardiac tissue replacement.[27] Natural (e.g., OSSIX PLUS, Tutodent, Bio-Gide, and Chondro-Gide)[28] and synthetic materials have been used, isolated or in combination, to fabricate membranes using methods such as solvent casting, electrospinning, polyelectrolyte complexation, or compression molding.[29] Although intense research efforts have been devoted to develop functional membranes as scaffolds for tissue engineering, limited work has been focused on developing membranes that exhibit a level of biomimetic complexity more similar to the in vivo environment.

The formation of membranes at the interface between two aqueous solutions, one containing a megadalton polymer and the other small self-assembling molecules bearing opposite charge, was previously demonstrated.[4] The structure-property relationship of these kinds of membranes has been studied[5] and the effect of electric fields on the self-assembly process forming the membranes has been recently investigated.[30] Inspired by this remarkable self-assembling system, we propose here a single-step bottom-up (self-assembly) and top-down (soft lithography) fabrication technique to create hybrid multifunctional membranes that, in addition to displaying biomimetic nanofibers and biomolecular elements, exhibit specific surface topographies that can be easily modified to elicit desirable biological responses. We have selected the natural polymer hyaluronic acid (HA), an anionic polysaccharide typically found in the connective tissues of vertebrates, to drive the self-assembly of a multidomain peptide, previously proposed by Hartgerink and co-workers.[31] The resulting peptide/HA co-assembled membranes exhibited a hierarchical structure of nanofibers and surface microtopographies with various densities of RGDS. Furthermore, we investigate the effect of temperature, time, and experimental setup on the structural characteristics of the membranes.

2. Results and Discussion

The self-assembling building blocks used in this study were a positively charged multidomain peptide, with or without the arginine-glycine-aspartic acid-serine (RGDS) cell-adhesive peptide sequence, and a high molecular weight (2 MDa) negatively charged biopolymer. The peptides, $K_2(QL)_6K_2$ and $K_2(QL)_6K_2$RGDS, were synthesized and purified successfully (MS and HPLC spectra provided in the supporting information). The multidomain $K_2(QL)_6K_2$ peptide (**Figure 1**A) consists of an ABA block motif[31] comprising a central block of glutamine-leucine (QL) repeats and two flanking positively charged lysines (K). Different variations of these multidomain peptides[32,33] have been previously synthesized and demonstrated to self-assemble into well-defined nanofibers[31] with various bioactive epitopes.[33,34] On the other hand, HA (Figure 1B) was selected due to its intrinsic polyanionic nature, linear unbranched random-coil structure, biocompatibility, low immunogenicity, and large size.[35] Furthermore, its presence in the natural ECM of many tissues and role in cellular signaling and wound healing makes it a highly attractive molecule to serve as a building block of a self-assembled biomimetic scaffold.

2.1. Fabrication of Smooth Membranes

When the $K_2(QL)_6K_2$ peptide solution (1 wt%) was added at a 1:1 ratio (v/v) to the high molecular weight hyaluronic acid solution (1 wt%), a membrane was obtained at the interface between the two solutions. However, the order in which the two solutions were combined (HA over the peptide or vice-versa) resulted in strikingly different types of membranes (**Figure 2**, **3**). Furthermore, time and temperature variations during the self-assembly and incubation of the membranes were also investigated and resulted in significant variations.

As expected, adding the viscous HA solution to the top of the peptide solution enabled the continuous growth of a self-assembled membrane, with its thickness increasing over time from 4 to 24 h after initial contact (Figure 2). This time-dependency is consistent with that reported by Capito et al. when mixing HA with a different self-assembling peptide.[4] When the HA solution was positioned on top of the peptide, 4 h after initial contact, the membranes exhibited an increase in thickness from 4 °C (9.37 ± 0.064 μm) up to 21 °C (15.55 ± 0.70 μm) to 50 °C (16.34 ± 1.40 μm) (Figure 2B). A similar increase was observed 24 h after contact from 4 °C (13.06 ± 2.99 μm) to 21 °C (26.84 ± 11.48 μm), but not from 21 to 50 °C (22.82 ± 11.21 μm). In addition, SEM observations revealed distinct surface morphologies on both sides of the membrane depending on the temperature. The surface of the HA-side at 4 °C (Figure 2A3) exhibited a higher heterogeneity associated with the presence of HA aggregates compared to the HA-side of membranes at 21 °C (Figure 2A7). This increase in surface homogeneity of the HA side and membrane thickness from 4 to 21 °C may be

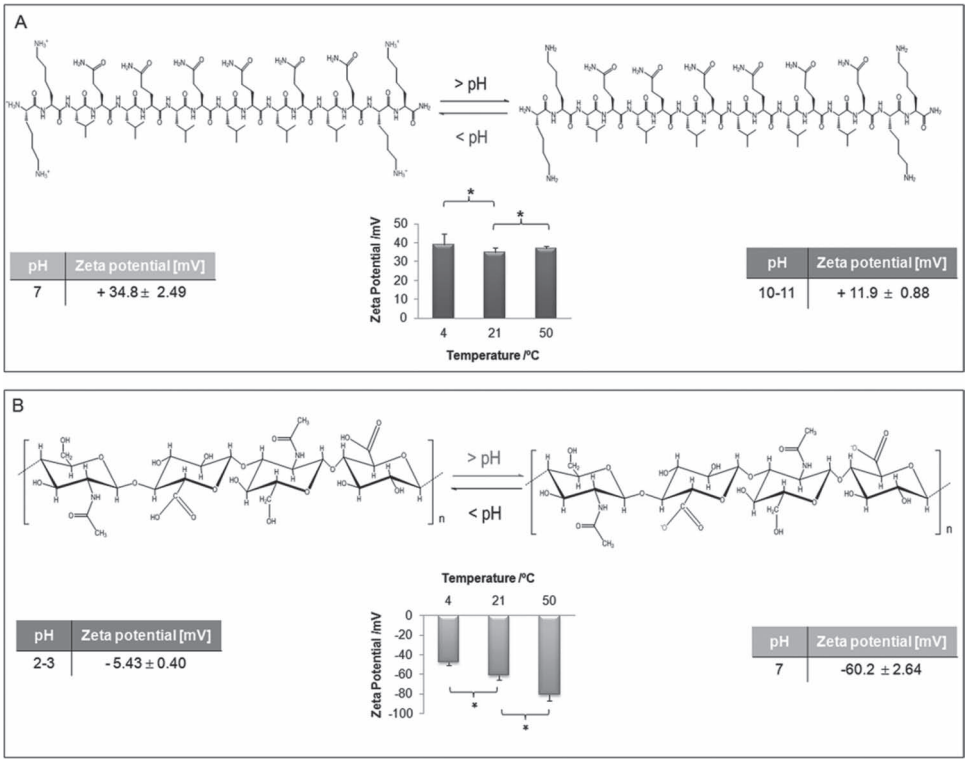

Figure 1. Chemical structure of the self-assembling components used in this study: multidomain $K_2(QL)_6K_2$ peptide (A) incorporating alternating hydrophilic/hydrophobic amino acid residues (QL) and two flanking positively charged lysines (K) required for self-assembly in presence of negatively charged high molecular weight polymer hyaluronic acid (B). Zeta potential of both component solutions (0.1 wt%) was measured at different temperatures and pH values to demonstrate the nature of ionizable groups in the self-assembling components (∗ indicates a significant difference ($p < 0.05$) between conditions).

a result of better diffusion and consequent enhanced interaction between HA and peptide molecules owing to the higher temperature during the self-assembly. Furthermore, confocal microscopy of membranes assembled with a fluorescently tagged HA enabled visualization of the distribution of HA through the membrane cross-section. The images in Figure 2C show that membranes assembled at 4 °C exhibited less fluorescence, suggesting an incomplete mixing of the components due to restricted mobility of the HA at lower temperatures. At 50 °C (data not shown), the membranes presented similar surface morphology and statistically similar thickness to those obtained at 21 °C, supporting our hypothesis.

Assuming the significance of electrostatic interactions on the self-assembly of the $K_2(QL)_6K_2$ peptide, we investigated the zeta potential of HA and peptide solutions at the different temperatures. It was found that at neutral pH the zeta potential of the peptide tended to decrease with an increase in temperature from 4 to 21 °C (Figure 1A, from 21 to 50 °C no significant change was observed), while the value for hyaluronic acid increased considerably across the whole temperature range (Figure 1B). The zeta potential is associated with the stability of charged aggregates in solution, and in this case should correlate to the total electrostatic charge of the molecules.[4] The greater values of the zeta potential obtained at higher temperatures, may indicate that at 21 and 50 °C the mobility of the HA chains is increased, allowing better diffusion of the two components into each other, resulting in the thicker and more robust membranes shown in Figure 2B. Similarly, Capito and co-workers[4] found that their self-assembled sacs were formed with greater physical integrity when both solutions had strong zeta potentials of opposite charge.

In addition to temperature and time, the experimental setup (e.g., peptide solution cast on top of HA solution or vice-versa), played a crucial role in the surface and cross-section morphology of the assembled membranes. When the peptide solution was positioned on top of the more viscous HA solution, a thin film was initially formed at the interface between the components, due to limited diffusion of the peptide into the viscous HA solution. This phenomenon would be accentuated at 4 °C because of the further reduction in mobility of the molecules, resulting in a membrane with two distinct layers (**Figure 3**A1). The bilayer membrane obtained at 4 °C was confirmed by confocal microscopy, where a dense layer of fluorescent HA can be distinguished from a darker region attributed to the peptide layer (Figure 3C). When the temperature was increased to 21 °C, although the presence of nano-fibers was observed, confirming a degree of self-assembly had occurred; HA fragments could still be seen on one side of the membrane (Figure 3A7).

These results show that it is possible to form both membranes made up of a single uniform layer and those consisting

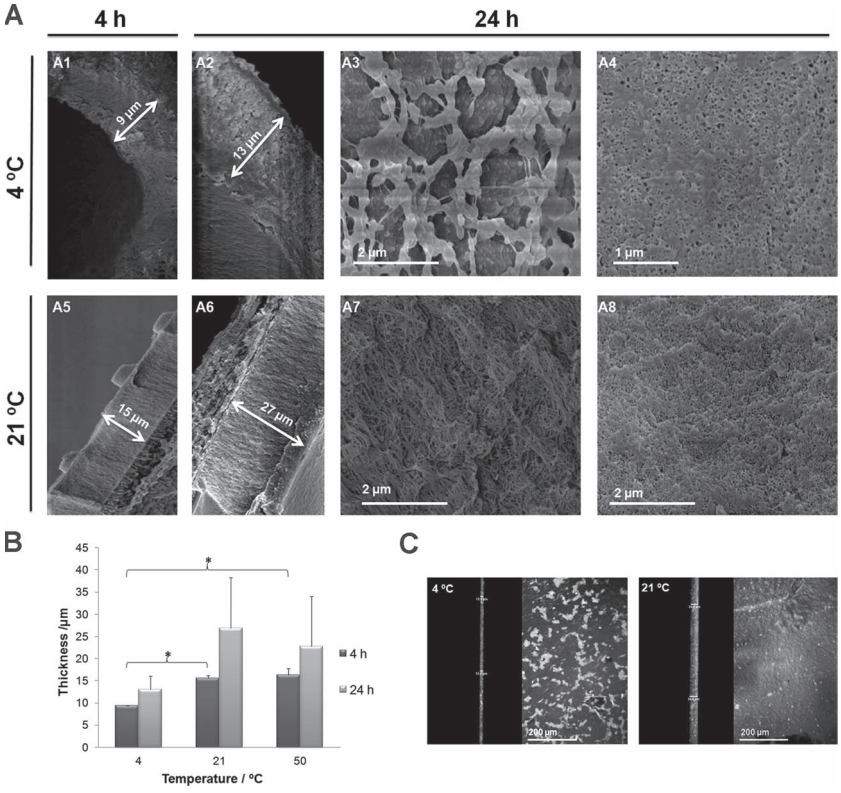

Figure 2. SEM images of membranes fabricated with hyaluronic acid on top of the peptide solution showing the membrane cross-sections at 4 °C (A1,A2) and 21 °C (A5,A6) after 4 and 24 h of incubation and surface morphology on the HA side (A3,A7) and peptide side (A4,A8). B) The increase in membrane thickness, measured by SEM, with increasing time and temperature (* indicates a significant difference ($p < 0.05$) between conditions). C) Confocal microscopy images of the membranes with fluorescein-HA formed after 4 h of incubation showing the distribution of fluorescent labeled HA over the membrane as well as the increase in membrane thickness with temperature.

of a bilayer with a peptide-rich side and a HA-rich side, by simply altering the experimental setup. This adds further versatility to the membranes, which expands the range of applications that they could potentially be used for.

2.2. Topographically Patterned Membranes

The 2D patterning of self-assembling peptides has been previously described in the literature.[36] Mata et al.[11] proposed a 3D patterning method applied to peptide amphiphiles that resulted in substrates capable of enhancing osteoblastic differentiation of MSCs. However, this fabrication process required further chemical modification of the peptide to enable photo-crosslinking in order to form the desired patterns. More recently, we reported on a drop casting/evaporation technique to create thin bioactive membranes based on recombinant elastin-like polymers.[13] While this process allowed the generation of self-supporting structures and the incorporation of both physical and biomolecular signals, it also required chemical cross-linking and lacked the biomimetic nanofibrous architecture. The present study aimed to overcome these limitations by relying solely on molecular co-assembly and soft lithography, resulting in precise biomimetic nanofibers, bioactive microtopographies, and self-supporting macroscopic membranes. Considering the lower resistance provided by the peptide solution (less viscous) to the diffusion of the HA molecules, we decided to cast first the peptide solution onto the hydrophilic patterned PDMS in order to guarantee that the solution would fill all the spaces in the molds, which in turn can guide their self-assembly, resulting in effective transference of the patterns (**Figure 4**C). Using this approach, membranes displaying posts (**Figure 5**A,D), holes (Figure 4D and Figure 5E), channels (Figure 5C), and pores (Figure 5F) ranging from 10 to 20 µm in lateral dimension were successfully produced. Figure 5B shows an image of the cross section of a membrane demonstrating the absence of distinct regions. The fabrication of patterned membranes with the peptide cast on top of the HA was also attempted, however the structures exhibited distortions and the quality was considerably inferior. In this case, the use of a top mold to press the setup from above may be necessary to improve the lithographic process.

Control of membrane thickness is recognized as being of extreme importance in the application of bioengineered scaffolds for tissue engineering applications.[37] We show here that it is possible to vary membrane thickness by changing the time and/or temperature during the molecular co-assembly process. Moreover, the membrane complexity can be increased by the combination of top-down and bottom-up methodologies. Examples of this have previously been reported in the literature,[11,13] however, for the membranes presented in this work, the topographical patterns are incorporated into the membrane structure during the self-assembly process. The versatility of these membranes to incorporate a variety of geometrical shapes is of extreme relevance, as it opens up the possibility to include specific physical signals that can be tailored to the specific application and designed to interact with cells on different length scales. Reproducible patterns were obtained over large regions of the membranes, which is a major criterion in the development of tissue engineered scaffolds, where sizeable surface areas are desirable for enhancing cell interactions.[13]

2.3. Biological Assessment

In order to investigate the effects of the physical guidance provided by topographies and the biomolecular signaling by the incorporated RGDS, rat mesenchymal stem cells (rMSCs) were cultured on the membranes. The difference in cell adhesion on the HA side versus the peptide side for smooth membranes was analyzed. In addition, the effect of different proportions of the RGDS sequence within the peptide component of the

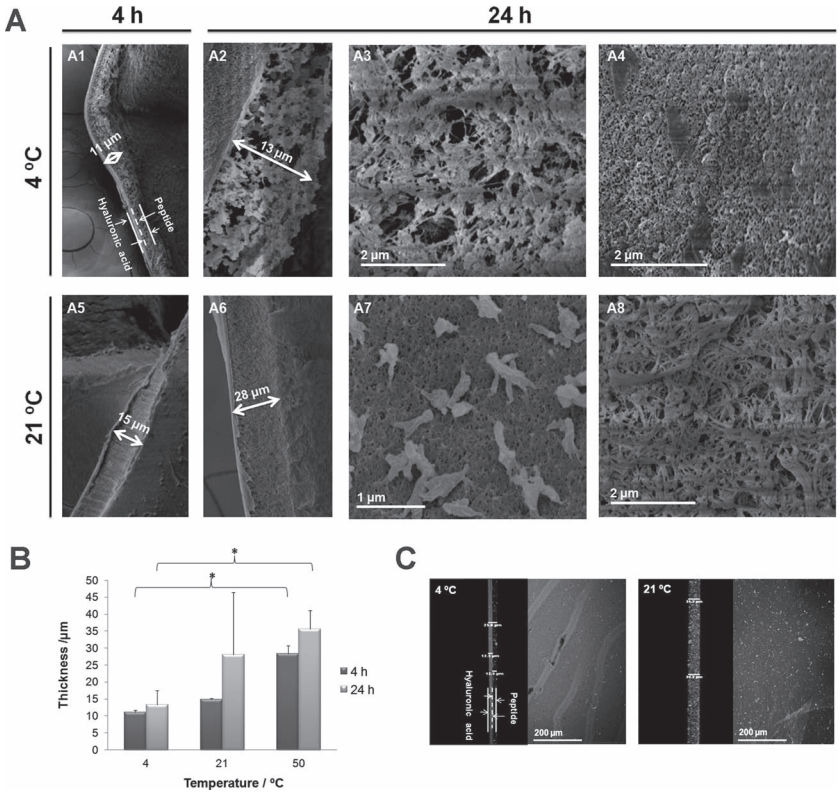

Figure 3. SEM images of membranes fabricated with peptide on top of hyaluronic acid solution showing the membrane cross-sections at 4 °C (A1,A2) and 21 °C (A5,A6) after 4 and 24 h of incubation and surface morphology on the HA side (A3,A7) and peptide side (A4,A8). B) The increase in membrane thickness, measured by SEM, with increasing time and temperature (* indicates a significant difference ($p < 0.05$) between conditions). C) Confocal microscopy images of the membranes with fluorescein-HA formed after 4 h of incubation showing the distribution of fluorescent labeled HA over the membrane as well as the increase in the membrane thickness with temperature.

membranes was assessed, as well as, the effect of the topographical patterns.

Rat MSCs were observed to adhere to both sides of the membrane, as well as to interact with the RGDS-containing peptide nanofibers, as shown in **Figure 6** and **7**. Without the RGDS cell binding sequence, the cells remained round without a visible actin cytoskeleton, appearing similar on both sides of the membrane (Figure 6A,D). However, for the membranes containing 10% RGDS motif rMSCs tended to attach and spread when cultured on the peptide side (Figure 6B). In contrast, on the HA side they maintained a rounded morphology (Figure 6E) and a lower number of attached cells were evident. For the membranes prepared with 30% RGDS, a large number of well-spread cells can be observed on the peptide side. Moreover, on the HA side there was a slight increase in the degree of spreading of the cells cultured in comparison to the membranes without RGDS or those with only 10% (Figure 6F). This indicates that a small quantity of the peptide solution diffused completely through the HA during the assembly process, and due to the high RGDS concentration in this instance, the proportion of the adhesion motif displayed on the HA surface was high enough to facilitate cell attachment. This is corroborated by the SEM images of the membranes formed under the same conditions, where a uniform single layer is evidence of extensive mixing of the two molecules (Figure 2). Although HA has previously been considered as a mediator of cell adhesion,[38] it is clearly not as effective as the RGDS sequence. It has been demonstrated that a number of cell-surface integrins have the ability to recognize the RGD peptide sequence,[39] and there is a great deal of evidence showing strong cell adhesion to substrates displaying this peptide motif, as has been demonstrated in the present study. This particular peptide motif was used in this work as a proof of principle. However, owing to the peptide molecular design, it would be extremely easy to incorporate an alternative signaling sequence in order to elicit more specific cellular responses.

It is well known that cell morphology can not only be modulated by epitope availability, but that physical signaling provided by topographical surface patterns can also have a noticeable effect. In this work, rMSCs were cultured on smooth and patterned membranes and their morphologies were assessed. In Figure 7, SEM images show that cells on the smooth membrane were randomly oriented. In contrast, when cells were seeded on membranes patterned with channels, they tended to align and spread along them, growing both on the ridges and within the channels. Cells also adapted their morphology when cultured on posts or holes. Similar behavior was observed by Tejeda and co-workers when culturing rMSCs on elastin like-polymer (ELP) membranes[13] with patterned channels. Figure 7 also contains high magnification images showing the cell filopodia attached to the membrane fibers.

These results confirm the potential of combining both biomolecular and physical features to act synergistically to elicit specific biological responses, such as cell proliferation or differentiation. Moreover, we have produced a membrane intrinsically containing these properties: fibrilar nanostructure (as a result of self-assembly), epitope availability (biomolecular signals), and micropatterns (topographic signals). The fabrication process for producing these membranes enables each of these features to be incorporated in a single step, without the need for additional chemical modifications of the molecules or post-assembly treatments.

3. Conclusions

In summary, a self-supporting bioactive membrane was produced through the self-assembly of a positively charged multidomain peptide triggered by a negatively charged high molecular weight polymer. The growth and structure of the membranes were seen to be affected by assembly time and temperature in addition to the positioning of components (peptide on top or bottom of HA). A biomolecular signaling motif was incorporated

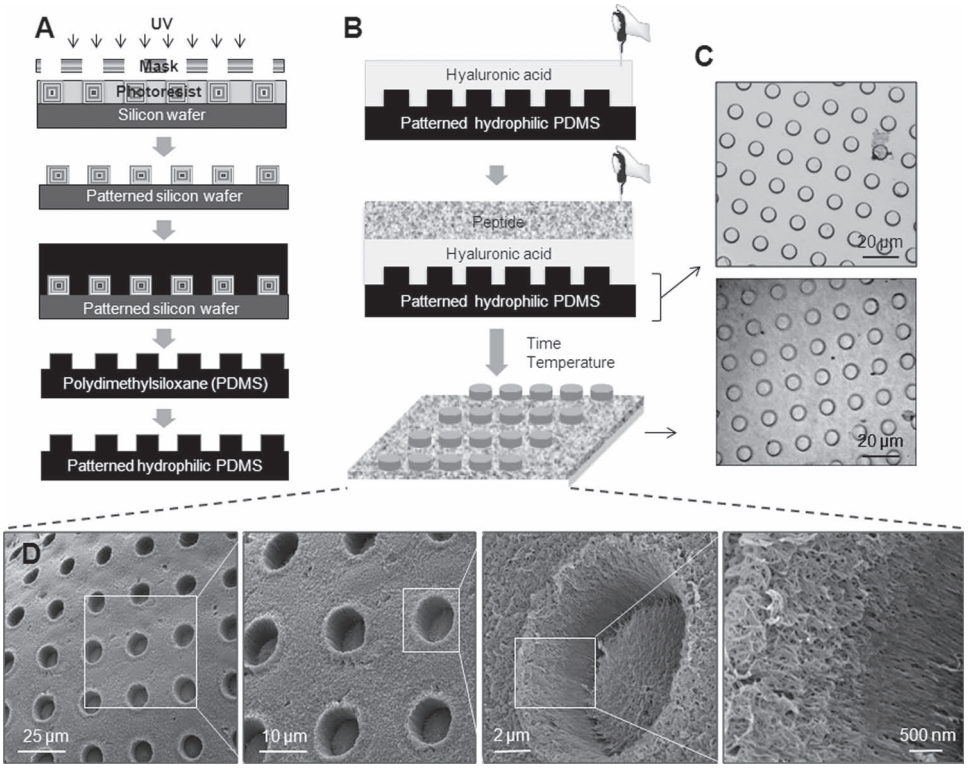

Figure 4. A) SU8-10 photoresist-coated Si wafer patterned by photolithography and the following steps of the microfabrication process. B) Membrane fabrication over the patterned PDMS mold. C) Images obtained by bright field microscopy of the patterned PDMS mold and patterned peptide–HA membrane after removal from the mold confirming the success of the transference of the patterns. D) SEM images and zoom-in of the patterned membrane surface demonstrating the fibrilar network resulting from the self-assembly of the $K_2(QL)_6K_2$ peptide triggered by HA.

into the membranes, and the proportion of this could be easily controlled by varying the composition of the peptide solution prior to assembly. Topographical features could be incorporated into the membrane structure during its formation, removing the requirement for post-assembly fabrication steps. Rat MSCs were observed to recognize the RGDS cell adhesion sequence and the topographical patterns, varying their morphology depending on the concentration of binding motif or specific physical features that were cultured on. The simultaneous integration of bottom-up and top-down fabrication

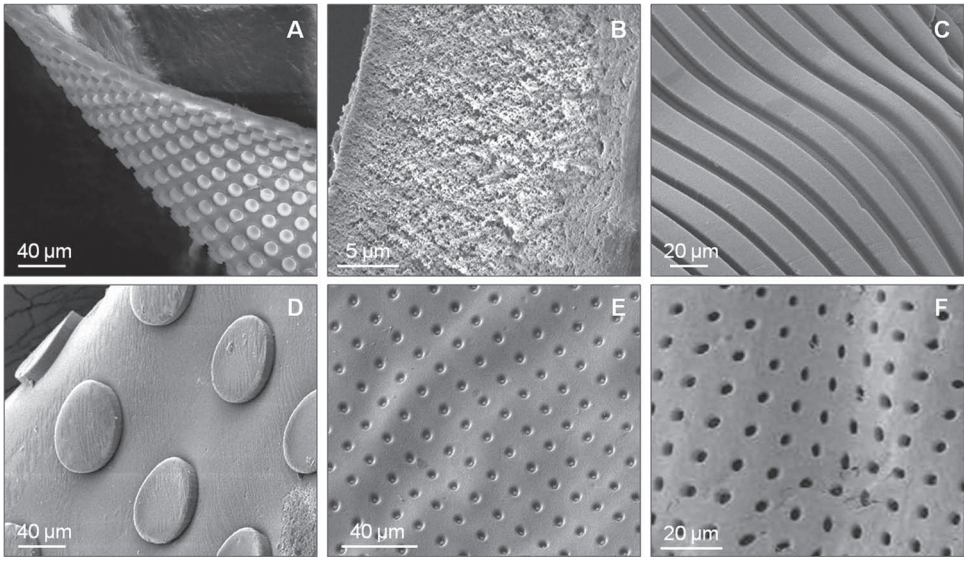

Figure 5. SEM images showing membranes with different patterned geometries: posts A) 10 and D) 20 μm in diameter, C) channels, E) pits 5 μm in diameter, F) pores 5 μm in diameter. Panel (B) shows an image of a membrane cross-section confirming the absence of distinct regions.

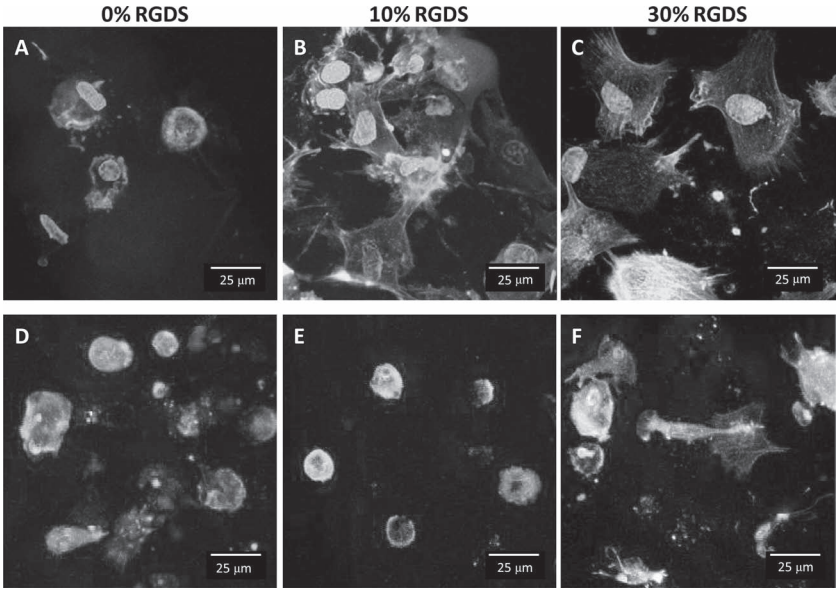

Figure 6. Confocal microscopy images showing the actin cytoskeleton and nuclei of rMSCs cultured for 18 h on the surface of smooth membranes with different percentages of RGDS: A–C) peptide side, D–F) hyaluronic acid side. A,D) no RGDS, B,E) 10% RGDS, and C,F) 30% RGDS.

processes described here permit the development of hierarchical macrostructures made from well-defined nanofibers and microtopographies that together provide precise biomolecular and physical properties. The numerous possibilities to better tune them with spatio-temporal and biomimetic control provide a broad spectrum of potential applications in tissue engineering and regenerative medicine.

4. Experimental Section

Peptide Synthesis and Purification: Two similar peptides were synthesized in this study, having the following amino acid sequences: $K_2(QL)_6K_2$ and $K_2(QL)_6K_2$RGDS. The structure of $K_2(QL)_6K_2$ is shown in Figure 1A. The peptides were produced by solid-phase peptide synthesis using standard 9-fluorenylmethoxycarbonyl (Fmoc) chemistry on an automated peptide synthesizer (CS Bio, USA) at 1 mmol scale on a 4-methylbenzhydrylamine (MBHA) rink amide resin. Fmoc-protected amino acids and MBHA rink amide resin were purchased from Novabiochem (USA) and O-(benzotriazol-1-yl)-*N*,*N*,*N*′,*N*′-tetramethyluronium (HBTU) from Carbosynth (UK). *N*-*N*-diisopropylethylamine (DIEA), piperidine and all other reagents were obtained from Sigma-Aldrich (USA). Once synthesized, cleavage of the peptide from the resin and deprotection of the protecting groups was carried out with a mixture of trifluoroacetic acid (TFA)/triisopropylsilane (TIS)/water (95/2.5/2.5) for 3 h at room temperature. After filtration of the cleavage mixture, excess TFA was removed by rotary evaporation. The resulting viscous peptide solution was triturated with cold diethylether. The white precipitate was collected by filtration, washed with cold ether, and allowed to dry under vacuum overnight. The peptide mass was confirmed by electrospray ionization mass spectrometry (ESI-MS, Finnigan LXQ, USA). The peptide was then purified on a Waters 2545 Binary Gradient high-performance liquid chromatography (HPLC) system using a preparative reverse-phase C18 column (Atlantis Prep OBD T3 Column, Waters) and a water/acetonitrile (0.1% TFA) gradient. TFA counter-ions were exchanged by sublimation from hydrochloric acid (0.1 M). Finally, the peptides were dialyzed against deionized water using dialysis tubing (500 MWCO, Spectrum Europe B.V., The Netherlands) to remove salts, lyophilized, to obtain a fluffy powder, and stored in closed containers at –20 °C until use. The purity and accurate mass of each peptide were verified using liquid chromatography/MS and the HPLC and mass spectra are given in the Supporting Information.

Zeta Potential Analysis: Zeta potential measurements of the peptide and hyaluronic acid (2 MDa, Lifecore Biomedical, Inc, USA) solutions (0.1 wt%) were performed at distinct pHs (T = 21 °C) and different temperatures (pH 7) using a Zetasizer Instrument (NANO-ZS ZEN3600, Malvern Instruments, UK).

Membrane Fabrication: Smooth membranes were fabricated by casting hyaluronic acid solution (2 MDa, 1 wt% in water) on a polydimethylsiloxane (PDMS, Sylgard 184, Dow Corning, USA) substrate. The PDMS substrate was prepared by mixing the prepolymer and crosslinker at a 10:1 ratio, degassing for 10 min under vacuum and curing for 2 h at 65 °C. The PDMS was oxygen plasma treated in a plasma cleaner (PDC-002, Harrick Cientific Corporation, USA), in order to increase the wettability of the surface. The $K_2(QL)_6K_2$ peptide (1 wt% in water) was next added on top of the HA, generating a membrane upon contact between the solutions. The membrane was allowed to age for either 4 or 24 h at 4, 21, and 50 °C. The membranes were also prepared inverting the positions of the HA and peptide: peptide solution was cast onto the PDMS substrate with the HA added on top. The effects of time and temperature on the membranes were also analyzed. Membranes containing different amounts of the RGDS motif were prepared by mixing the $K_2(QL)_6K_2$ and $K_2(QL)_6K_2$RGDS peptides in different ratios (1:10 and 3:10) prior to the co-assembly with HA.

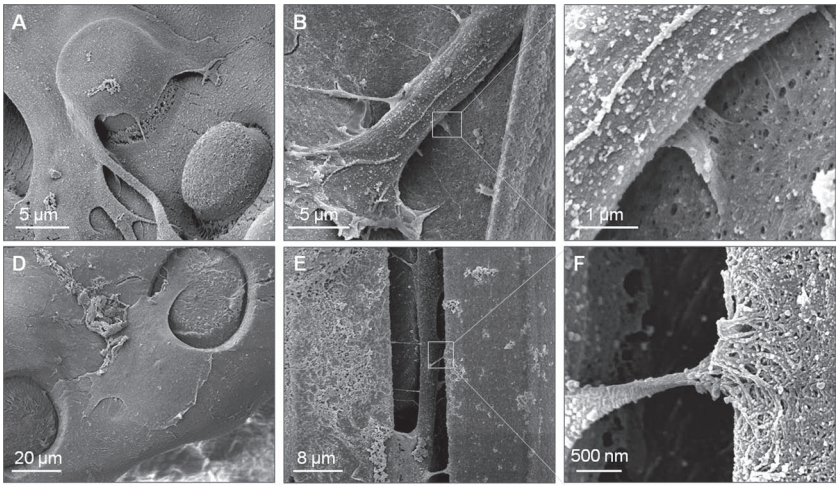

Figure 7. SEM images showing differences in cell morphology when cultured on smooth membranes and those patterned with different topographies: A) posts 10 μm in diameter; B,C) smooth; D) holes 20 μm in diameter; and E,F) channels 10 μm across.

Topographically Patterned Membrane Fabrication: Fabrication of Topographic PDMS Molds: Molds composed of several microtopographical patterns

were fabricated using a soft lithography process. The patterns were generated in SU8-10 photoresist (Microchem Corporation, USA) using conventional contact mode UV photolithography (Mask Aligner MJB4, SUSS Microtec, Germany) with a rigid chrome mask as follows. SU8-10 photoresist was spin coated onto a (111)-oriented silicon wafer (Siltronix) at 500 rpm for 5 s followed by 4000 rpm for 30 s, achieving a layer approximately 8 μm thick. The sample was baked at 65 °C for 2 min and 95 °C for 5 min prior to UV exposure (3.3 s at 30 mW cm^{-2}) and baked post-exposure at 65 °C for 1 min followed by 95 °C for 5 min. The topographical patterns were then developed with SU8 developer (Microchem, USA). The resulting samples were silanized with trichloro(1*H*,1*H*,2*H*,2*H*-perfluorooctyl)silane (Sigma-Aldrich, USA) before being used as molds for the production of patterned PDMS substrates (Figure 4A). The patterns were comprised of different geometries, channels (10 μm wide, 10 μm in separation, and 8 μm in height), posts (10 μm wide, 10 μm in separation, and 8 μm in height), and holes (10 μm wide, 10 μm in separation, and 8 μm deep), and posts and holes (20 μm wide, 20 μm in separation, and 8 μm in height).

Fabrication of Topographic Membranes: Topographically patterned membranes were fabricated by casting the peptide solution onto the hydrophilic PDMS molds followed by the addition of the HA on the top of peptide solution (Figure 4-B). The membranes were aged for 24 h at room temperature. The self-assembled membranes were removed from the patterned PDMS molds by immersion in ethanol (70%) and then characterized.

Membrane Characterization: Scanning Electron Microscopy (SEM): The morphology and uniformity of membrane surface and cross-section were investigated by SEM. Prior to the SEM observations, the membranes were fixed with glutaraldehyde (Electron Microscopy Sciences, Spain) solution (2.5%, v/v in 0.1 M phosphate buffer solution, pH 7.4) for 1 h. The samples were then dehydrated in a graded ethanol series (50, 70, 90, 96 and 100%) followed by immersion in hexamethyldisilazane (HMDS, Sigma-Aldrich, Spain). The membranes were sputter-coated with 20 nm of gold and then visualized using a Nova nano SEM (FEI, Netherlands).

Confocal Microscopy: To get better insight into the self-assembly process, namely on the mixture of the components during membrane formation, HA was labeled with 5-(aminoacetamido) Fluorescein (Life Technologies, USA) according to a procedure described elsewhere.[40] The membranes were prepared as described previously, with variations in time, temperature and positioning of peptide and fluorescent HA. They were then imaged using an SP2 confocal microscope (Leica Microsystems, Germany).

Biological Assessment: Cell Seeding and Culture on the Fabricated Membranes: Rat mesenchymal stem cells (rMSCs) isolated from bone marrow of rat tibia and femur, were provided by the Animal Research Center (SEA) of the Parc Científic Barcelona. Cells were expanded in Dulbecco's modified Eagle's medium (DMEM; Life Technologies, Spain) supplemented with fetal bovine serum (10%, FBS; Attendbio Research, Spain), L-glutamine (0.2 mM), penicillin (100 units mL^{-1}) and streptomycin (0.1 mg mL^{-1}) (Sigma-Aldrich, Spain). rMSCs of passage 3–6 were suspended in serum-free DMEM and seeded at 12 500 cells cm^{-2} onto smooth and patterned membranes with and without the RGDS sequence. After 4 h of culture, all medium was replaced with DMEM containing 10% FBS to allow cell proliferation.

Cell Adhesion: After 18 h, the culture medium was removed and the samples were washed twice with PBS to remove any non-adherent cells. Cells were fixed with formaldehyde (4%, v/v, Sigma-Aldrich, Spain) in PBS for 30 min at RT. To visualize the actin cytoskeleton, cells were stained with phalloidin-fluorescein isothiocyanate (phalloidin–FITC, Sigma-Aldrich, Spain) at a 1:500 dilution in PBS for 1 h at room temperature. They were then counterstained with 4′,6-diamidino-2-phenylindole dihydrochloride (DAPI; Sigma-Aldrich, Spain) for observation of the nuclei. Finally, the samples were mounted on glass slides with a drop of Fluoro-Gel mountant (Aname, Spain). The cells were visualized using an SPE confocal microscope (Leica Microsystems, Germany).

SEM Observations: Cells cultured on the membranes were examined under SEM to analyze cell morphology and its interactions with the membranes at the nano and microscale. Samples were fixed and dehydrated as described above.

Statistical Analysis: The results of zeta potential and membrane thickness are expressed as a mean ± standard deviation with $n = 3$ for each condition. Statistical significance of differences was determined using the unpaired Student's t-test multiple comparison procedure at a confidence level of 95% ($p < 0.05$).

Supporting Information

Supporting Information is available from the Wiley Online Library or from the author.

Acknowledgements

Funding for this study was provided by the Portuguese Foundation for Science and Technology (FCT, grant PTDC/EBB-BIO/114523/2009), the Ministry of Science and Innovation (MICINN) of the Government of Spain, and the Parc Cientìfic Barcelona. A.C.M. gratefully acknowledges FCT for providing a PhD grant (SFRH/BD/42161/2007). Some additional support for this work was obtained from Bilateral Program Portugal-Spain Integrated Actions 2011 (E-50/11). The authors thank Daniela Ferreira from the 3B's Research Group at the University of Minho for her assistance with mass spectrometry analysis and Marina Cazorla from The Nanotechnology Platform, Parc Cientific Barcelona for her support related with the microfabrication.

Received: April 17, 2012
Published online: September 3, 2012

[1] C. Sanchez, H. Arribart, M. M. G. Guille, *Nat. Mater.* **2005**, *4*, 277.
[2] N. Huebsch, D. J. Mooney, *Nature* **2009**, *462*, 426.
[3] L. E. R. O'Leary, J. A. Fallas, E. L. Bakota, M. K. Kang, J. D. Hartgerink, *Nat. Chem.* **2011**, *3*, 821.
[4] R. M. Capito, H. S. Azevedo, Y. S. Velichko, A. Mata, S. I. Stupp, *Science* **2008**, *319*, 1812.
[5] D. Carvajal, R. Bitton, J. R. Mantei, Y. S. Velichko, S. I. Stupp, K. R. Shull, *Soft Matter* **2010**, *6*, 1816.
[6] L. W. Chow, R. Bitton, M. J. Webber, D. Carvajal, K. R. Shull, A. K. Sharma, S. I. Stupp, *Biomaterials* **2011**, *32*, 1574.
[7] W. J. Chung, J. W. Oh, K. Kwak, B. Y. Lee, J. Meyer, E. Wang, A. Hexemer, S. W. Lee, *Nature* **2011**, *478*, 364.
[8] K. H. Smith, E. Tejeda-Montes, M. Poch, A. Mata, *Chem. Soc. Rev.* **2011**, *40*, 4563.
[9] Y. N. Xia, G. M. Whitesides, *Annu. Rev. Mater. Sci.* **1998**, *28*, 153.
[10] Z. H. Nie, E. Kumacheva, *Nat. Mater.* **2008**, *7*, 277; M. Park, C. Harrison, P. M. Chaikin, R. A. Register, D. H. Adamson, *Science* **1997**, *276*, 1401.
[11] A. Mata, L. Hsu, R. Capito, C. Aparicio, K. Henrikson, S. I. Stupp, *Soft Matter* **2009**, *5*, 1228.
[12] A. Mata, E. J. Kim, C. A. Boehm, A. J. Fleischman, G. F. Muschler, S. Roy, *Biomaterials* **2009**, *30*, 4610.
[13] E. Tejeda-Montes, K. H. Smith, M. Poch, M. J. Lopez-Bosque, L. Martin, M. Alonso, E. Engel, A. Mata, *Acta Biomater.* **2012**, *8*, 998.
[14] a) A. I. Teixeira, G. A. Abrams, P. J. Bertics, C. J. Murphy, P. F. Nealey, *J. Cell Sci.* **2003**, *116*, 1881; b) A. I. Teixeira, G. A. McKie, J. D. Foley, P. J. Berticsc, P. F. Nealey, C. J. Murphy, *Biomaterials* **2006**, *27*, 3945.
[15] H. G. Craighead, C. D. James, A. M. P. Turner, *Curr. Opin Solid State Mater. Sci.* **2001**, *5*, 177.
[16] A. Mata, C. Boehm, A. J. Fleischman, G. Muschler, S. Roy, *Biomed. Microdevices* **2002**, *4*, 267.

[17] A. Mata, C. Boehm, A. J. Fleischman, G. F. Muschler, S. Roy, *Int. J. Nanomed.* **2007**, *2*, 389.
[18] a) M. J. Dalby, N. Gadegaard, R. Tare, A. Andar, M. O. Riehle, P. Herzyk, C. D. W. Wilkinson, R. O. C. Oreffo, *Nat. Mater.* **2007**, *6*, 997; b) R. J. McMurray, N. Gadegaard, P. M. Tsimbouri, K. V. Burgess, L. E. McNamara, R. Tare, K. Murawski, E. Kingham, R. O. C. Oreffo, M. J. Dalby, *Nat. Mater.* **2011**, *10*, 637.
[19] G. J. Wang, C. C. Hsueh, S. H. Hsu, H. S. Hung, *J. Micromech. Microeng.* **2007**, *17*, 2000.
[20] K. Y. Suh, J. Seong, A. Khademhosseini, P. E. Laibinis, R. Langer, *Biomaterials* **2004**, *25*, 557.
[21] M. R. Steedman, S. L. Tao, H. Klassen, T. A. Desai, *Biomed. Microdevices* **2010**, *12*, 363.
[22] V. S. LeBleu, B. MacDonald, R. Kalluri, *Exp. Biol. Med.* **2007**, *232*, 1121.
[23] K. N. Malizos, L. K. Papatheodorou, *Injury* **2005**, *36*, 13.
[24] B. D. Lawrence, J. K. Marchant, M. A. Pindrus, F. G. Omenetto, D. L. Kaplan, *Biomaterials* **2009**, *30*, 1299.
[25] S. MacNeil, *Nature* **2007**, *445*, 874.
[26] C. Y. Shi, W. Chen, Y. N. Zhao, B. Chen, Z. F. Xiao, Z. L. Wei, X. L. Hou, J. Tang, Z. X. Wang, J. W. Dai, *Biomaterials* **2011**, *32*, 753.
[27] J. Gao, J. Z. Liu, Y. Gao, C. Wang, Y. N. Zhao, B. Chen, Z. F. Xiao, Q. Miao, J. W. Dai, *Tissue Eng., Part A* **2011**, *17*, 2739.
[28] P. H. Warnke, T. Douglas, S. Sivananthan, J. Wiltfang, I. Springer, S. T. Becker, *Clin. Oral Implants Res.* **2009**, *20*, 761.
[29] D. F. Stamatialis, B. J. Papenburg, M. Girones, S. Saiful, S. N. M. Bettahalli, S. Schmitmeier, M. Wessling, *J. Membrane Sci.* **2008**, *308*, 1.
[30] Y. S. Velichko, J. R. Mantei, R. Bitton, D. Carvajal, K. R. Shull, S. I. Stupp, *Adv. Funct. Mater.* **2012**, *22*, 369.
[31] H. Dong, S. E. Paramonov, L. Aulisa, E. L. Bakota, J. D. Hartgerink, *J. Am. Chem. Soc.* **2007**, *129*, 12468.
[32] L. Aulisa, H. Dong, J. D. Hartgerink, *Biomacromolecules* **2009**, *10*, 2694.
[33] K. M. Galler, L. Aulisa, K. R. Regan, R. N. D'Souza, J. D. Hartgerink, *J. Am. Chem. Soc.* **2010**, *132*, 3217.
[34] K. M. Galler, J. D. Hartgerink, A. C. Cavender, G. Schmalz, R. N. D'Souza, *Tissue Eng., Part A* **2012**, *18*, 176.
[35] D. D. Allison, K. J. Grande-Allen, *Tissue Eng.* **2006**, *12*, 2131.
[36] M. A. Biesalski, A. Knaebel, R. Tu, M. Tirrell, Biomaterials **2006**, *27*, 1259; D. Stroumpoulis, H. N. Zhang, L. Rubalcava, J. Gliem, M. Tirrell, *Langmuir* **2007**, *23*, 3849.
[37] B. E. Uygun, T. Bou-Akl, M. Albanna, H. W. T. Matthew, *Acta Biomater.* **2010**, *6*, 2126.
[38] M. Cohen, D. Joester, B. Geiger, L. Addadi, *ChemBioChem* **2004**, *5*, 1393.
[39] a) C. N. Salinas, K. S. Anseth, *J. Tissue Eng. Regener. Med.* **2008**, *2*, 296; b) J. E. Frith, R. J. Mills, J. J. Cooper-White, *J. Cell Sci.* **2012**, *125*, 317; c) E. Ruoslahti, *Ann. Rev. Cell Dev. Biol.* **1996**, *12*, 697.
[40] J. Gajewiak, S. Cai, X. Z. Shu, G. D. Prestwich, *Biomacromolecules* **2006**, *7*, 1781.